Annals of Nuclear Medicine Vol. 15, No. 4, 321–327, 2001

Is technetium-99m-MIBI taken up by the normal pituitary gland? A comparison of normal pituitary glands and pituitary adenomas

Toyoyuki KOJIMA, Sunao MIZUMURA, Shin-ichiro KUMITA, Tatsuo KUMAZAKI and Akira TERAMOTO

Departments of Neurosurgery and Radiology, Nippon Medical School

Purpose: The aim of this study was to compare the behavioral uptake of a normal gland and a pituitary adenoma and to assess the ability to diagnose pituitary adenoma by means of technetium-99m-hexakis-2-methoxy-isobutyl-isonitrile (MIBI) single photon emission computed tomography (SPECT).
Methods: The study included 15 patients with pituitary adenomas (mean age = 44.0 years, range 19–63) and 15 control subjects (mean age = 50.7 years, range 20–67). SPECT was performed 15 minutes after an intravenous injection of MIBI 600 MBq. The shape and location of MIBI uptake were evaluated on a magnetic resonance (MR) imaging/SPECT registration image. The shape patterns and location were classified as follows: Shape C (circular); LO (longitudinal oval); T/R (triangular or rectangular) and location P (pituitary gland or adenoma); D/C (dorsum sellae and/or clivus).
Results: Analysis of the uptake showed that 10 (67%) adenomas were C, and 5 (33%) were LO. Of the controls, 5 (33%) were C, and 10 (69%) were T/R. With regard to location, all patients with pituitary adenomas were classified as P, and all control subjects (93%) but one showed uptake in the dorsum sellae and clivus (D/C).
Conclusion: MIBI was taken up in the dorsum sellae or clivus but not the normal pituitary gland and had a strong affinity for the pituitary adenoma. This result implies that MIBI SPECT may be a useful new auxiliary examination technique for the location diagnosis of pituitary adenoma.

Key words: adenoma, pituitary gland, technetium-99m-MIBI

INTRODUCTION

^{99m}Tc-hexakis-2-methoxy-isobutyl-isonitrile (MIBI) is a fat-soluble cationic pharmaceutical preparation used for myocardial perfusion imaging and tumor imaging in the same way as ^{201}TlCl. MIBI has been proposed as a tracer for the detection of thyroid, parathyroid, lung, breast, bone and brain tumors.[1–6] The mechanism of ^{201}TlCl uptake in tumors is related to increased sodium-potassium adenosine triphosphate (ATPase) pump activity,[7,8] whereas MIBI accumulates within the mitochondria and cytoplasm of the cells. MIBI uptake depends on the potential difference between mitochondrial and plasma membranes.[9,10]

Although many studies of brain tumors by means of MIBI single photon emission computed tomography (SPECT) have been reported, there are few studies on pituitary adenomas.[11,12] MIBI uptake is reported to distribute to normal structures of the pituitary gland,[13] and also to the choroid plexus, salivary glands, nasopharynx,[14] and bone marrow.[15] Since the difference between the normal pituitary gland and pituitary adenoma in MIBI uptake behavior has never been clear, the aim of this study was to compare the uptake behavior of the two and to assess MIBI SPECT's ability to diagnose pituitary adenoma.

Received September 18, 2000, revision accepted April 18, 2001.

For reprint contact: Toyoyuki Kojima, M.D., Department of Neurosurgery, Nippon Medical School, 1–1–5 Sendagi, Bunkyo-ku, Tokyo 113–8603, JAPAN.
E-mail: toyoyuki@nms.ac.jp

Table 1 Clinical characteristics and SPECT/MRI findings

Normal pituitaries

Study No.	Age (yr)	Sex	Diagnosis	Shape	Location	Distance (mm)		Δ
						MRI	SPECT	
1	67	F	Metastatic brain tumor	C	D/C	67	75	8
2	43	M	Astrocytoma	C	D/C	69	77	8
3	59	F	Cerebellar glioma	C	D/C	64	69	5
4	30	M	Hemangioblastoma	C	D/C	67	71	4
5	55	F	Cushing syndrome (adrenal tumor)	C	D/C	73	78	5
6	54	M	Metastatic brain tumor	T/R	D/C	73	77	4
7	59	F	Metastatic brain tumor	T/R	D/C	70	74	4
8	61	M	Astrocytoma	T/R	D/C	70	78	8
9	62	F	Meningioma	T/R	D/C	63	68	5
10	51	M	Acoustic neurinoma	T/R	D/C	74	78	4
11	61	M	Malignant lymphoma	T/R	D/C	63	68	5
12	55	M	Thalamic glioma	T/R	D/C	73	80	7
13	32	F	Cavernous angioma	T/R	P	68	70	2
14	52	F	Intraventricular tumor	T/R	D/C	70	75	5
15	20	M	Sarcoidosis	T/R	D/C	74	80	6
Mean ± s.d.	50.7 ± 14					69.2 ± 3.8	74.5 ± 4.3	5.3 ± 1.8

Pituitary adenomas

Study No.	Age (yr)	Sex	Histological diagnosis	size (mm)	Shape	Location	Distance (mm)		Δ
							MRI	SPECT	
1	47	F	ACTHoma	8	C	P	69	72	3
2	57	M	GHoma	8	C	P	73	75	2
3	63	F	GHoma	9	C	P	74	76	2
5	23	F	PRLoma	9	C	P	62	64	2
6	20	F	PRLoma	9	C	P	62	64	2
4	51	M	NFoma	9	LO	P	75	75	0
8	49	M	GHoma	10	C	P	69	71	2
7	62	F	GHoma	10	LO	P	67	68	1
9	52	F	GHoma	16	C	P	73	72	−1
10	28	F	TSHoma	17	LO	P	68	70	2
11	35	F	PRLoma	24	C	P	68	71	3
12	31	M	PRLoma	25	C	P	70	73	3
13	19	F	PRLoma	26	C	P	65	68	3
14	60	M	NFoma	36	LO	P	70	69	−1
15	57	F	NFoma	48	LO	P	71	72	1
Mean ± s.d.	43.6 ± 16.0			17.6 ± 11.6			68.9 ± 4.1	70.6 ± 3.7	1.6 ± 1.4

GHoma = GH secreting adenoma; ACTHoma = ACTH secreting adenoma; PRLoma = PRL secreting adenoma; TSHoma = TSH secreting adenoma; NFoma = Non-functioning adenoma; C = Circular; LO = Longitudinal oval; T/R = Triangular- or recutangular-shape; P = Pituitary gland or adenoma; D/C = Dorsum sellae and/or clivus; Δ = SPECT-MRI (mm).

PATIENTS AND METHODS

The study involved 15 consecutive patients with pituitary adenomas (mean age = 43.6 years, range 19–63) and 15 control subjects (mean age = 50.7 years, range 20–67). Pituitary adenomas consisted of growth hormone (GH)-secreting adenomas (n = 5), non-functioning adenomas (n = 3), prolactin (PRL)-secreting adenomas (n = 5), adrenocorticotropic hormone (ACTH)-secreting adenomas (n = 1) and thyroid stimulating hormone (TSH) secreting adenomas (n = 1). All patients underwent transsphenoidal surgery and were diagnosed on the basis of hormonal and immunopathological findings. Control subjects included those with a brain tumor or suspected brain tumor unrelated to the sellar region and all had normal pituitary glands determined by MRI (magnetic resonance imaging). Informed consent was obtained from all the study subjects.

Magnetic Resonance imaging

MRI was done with a high-field-strength (1.5-T) imager (Sigma Horizon, General Electric, Milwaukee, WI) with gadolinium diethylenetriamine-pentaacetic acid (Gd-DTPA). The imaging parameters were as follows: repeti-

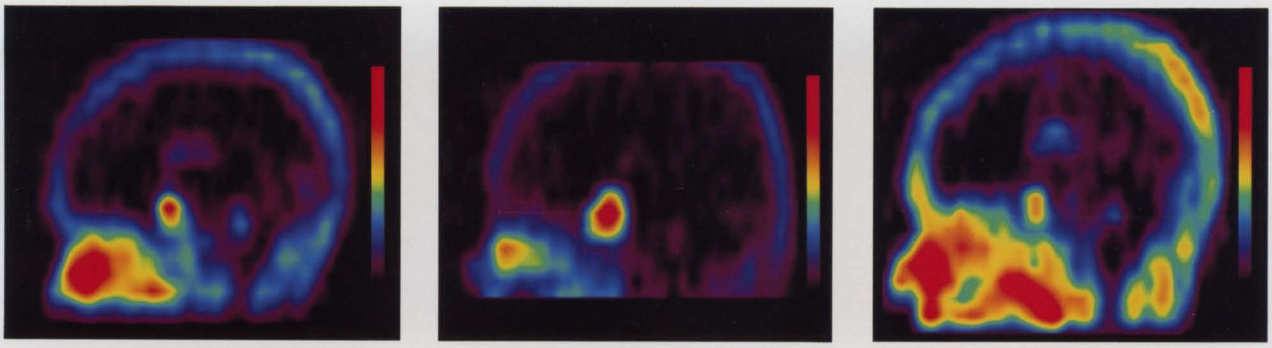

A B C

Fig. 1 Midsagittal SPECT image obtained 15 minutes after ^{99m}Tc-MIBI intravenous injection shows typical examples of the three patterns: A, B, and C demonstrate Circular, Longitudinal oval, and Triangular or rectangular shapes, respectively.

tion time (TR) 600 msec, echo time (TE) 20 msec, field of view 16–23 cm, image acquisition matrix 256×256, and section thickness 3.5 mm.

SPECT imaging

A SPECT scan of the brain was done 15 minutes after a 600 MBq intravenous injection of ^{99m}Tc-MIBI. Image data were acquired with a three-headed gamma camera (Prism 3000, Picker-Shimadzu, Co., Kyoto, Japan) equipped with high resolution, fan-beam collimators (full width at half maximum: FWHM = 8 mm). Projection data were accumulated in a 128×128 matrix, 45 sec/angle, 30 angles for each detector (4° steps, 120° rotation). Projection images were smoothed and reconstructed in a 128×128 matrix, with Metz-filtered (cut-off frequency 3.48 cycles/cm) back projection. Slice thickness was 4.45 mm.

Image analysis

1) SPECT imaging

The shape of MIBI uptake was evaluated for all the subjects on a midsagittal plane to allow for differentiation of the anteroposterior structures of the pituitary gland. The shape patterns were classified as follows:

C (circular), LO (longitudinal oval), and T/R (triangular- or rectangular-shape).

Figure 1 shows typical examples of the three patterns.

2) Registration imaging

To evaluate where MIBI accumulated in the parasellar region, a registration image was prepared by superimposing MRI and SPECT images. Each midsagittal plane was transferred to a UNIX workstation for adjustment of the enlargement ratio and was superimposed by matching anatomical characteristics such as the shape of the nose, calvaria, and skull base (registration image). With this image, the location of MIBI uptake was classified as follows:

P (pituitary gland or adenoma) and D/C (dorsum sellae and/or clivus).

One pituitary adenoma patient (study No. 2) was evaluated with not only a sagittal but also a coronal registration image because MRI and SPECT images revealed that the lesion was located on the left side of the midline. Two nuclear medicine physicians, who had been given no information about the subject's status, evaluated the shape and location.

Distance analysis

To identify the fitting errors of the registration image, the distance from the nasion to the parasellar region was measured by dedicated computers for both MR and SPECT images. The two distances (mm) from the nasion to the center of the pituitary gland or adenoma and to the dorsum sellae were measured on MRI, and the distance (mm) from the nasion (the most concave point between the forehead and nose relative to the skin surface) to the center of the parasellar uptake region was measured on the SPECT images for all the subjects. We evaluated the mean distance in each image, and an unpaired t-test was used for pituitary adenomas and normal pituitary glands. Significance was established at the $p < 0.05$ level.

RESULTS

Clinical characteristics and SPECT/MRI findings are summarized in Table 1. Of the 15 adenomas, 8 were microadenomas (maximal diameter < 10 mm) and 7 macroadenomas (maximal diameter ≥ 10 mm). The mean diameter of the adenomas was 17.6 mm (range, 8–48).

Image analysis

1) Of the 15 adenoma patients, 10 (67%) (8 microadenomas, 2 macroadenomas) were classified as shape C, 5 (33%) (0 microadenomas, 5 macroadenomas) shape LO, and none (0%) shape T/R. Of the 15 controls, 5 (33%) MIBI shape patterns were classified as C, none (0%) shape LO, and 10 (69%) shape T/R.

2) In the registration image, all 15 adenomas (100%) showed MIBI uptake at location P (Fig. 2). For the

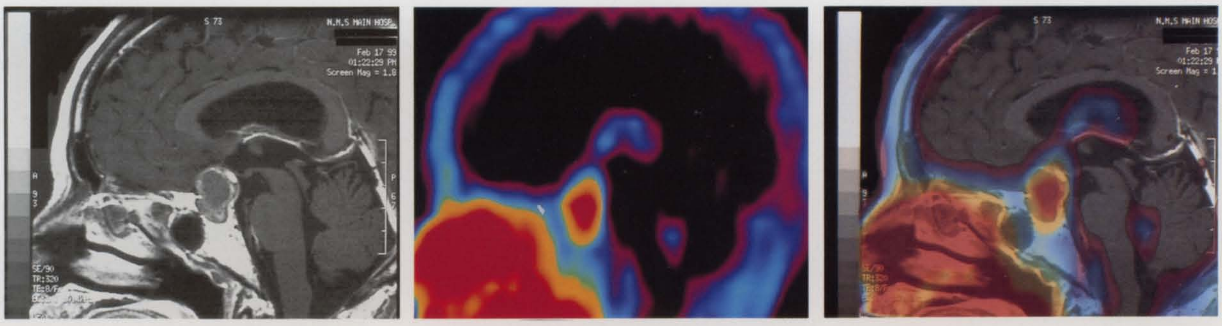

A B C

Fig. 2 A 57-year-old woman with non-functioning macroadenoma. T1-weighted sagittal image with contrast material (A), SPECT image (B), and the registration image (C). The registration image shows MIBI uptake in the whole adenoma (location P).

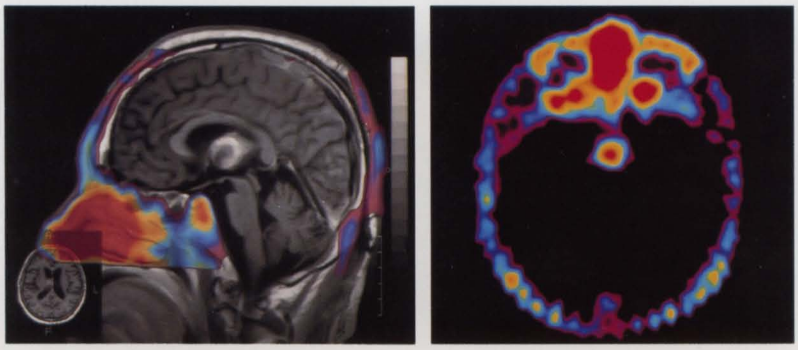

A B

Fig. 3 A 67-year-old man with metastatic brain tumor and normal pituitary gland. The registration image (A) shows MIBI uptake in the dorsum sellae and upper clivus (triangular shape and location D/C). However, in the SPECT transverse image (B), the parasellar uptake can not be distinguished from that in the normal pituitary gland.

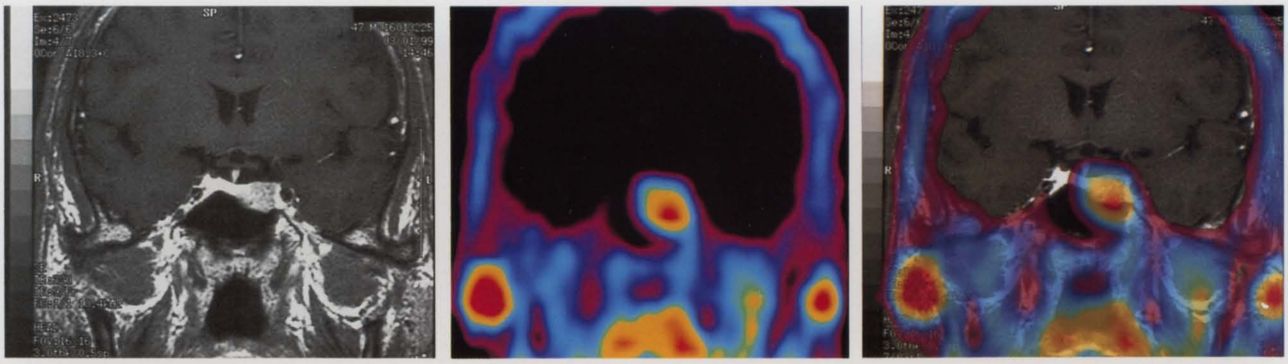

A B C

Fig. 4 A 57-year-old man with GH secreting microadenoma (location P). T1-weighted coronal MR image with contrast (A) revealed a pituitary adenoma on the left side and normal pituitary gland on the right side. MIBI SPECT coronal image (B) also demonstrated uptake on the left side. MIBI uptake in the registration image (C) was observed in the pituitary adenoma but not in the normal pituitary gland.

controls, 14 (93%) showed uptake at location D/C with the remaining one (7%) at location P (Fig. 3). The coronal image revealed that MIBI was not taken up in the normal pituitary gland but in the pituitary adenoma (Fig. 4).

Distance analysis

The mean distances determined with MRI from the nasion to the parasellar region for controls and pituitary adenomas were 69.2 ± 3.8 mm and 68.9 ± 4.1 mm, respectively, and 74.5 ± 4.3 mm and 70.6 ± 3.7 mm, respectively with SPECT. With MRI, no significant differences were found between the two groups. In contrast, the mean distances determined with the SPECT images between for the two groups were significantly different ($p < 0.01$, unpaired t-test). The mean uptake observed in the controls was located 3.8 mm behind that of the adenomas.

DISCUSSION

The diagnosis of pituitary adenoma is determined by MRI and by hormonal analysis. MRI has proved to be an accurate method for the evaluation of pituitary adenoma, and dynamic MRI has been used recently to detect microadenomas.[16] It is sometimes difficult, however, to pinpoint the lesion by means of anatomical imaging because of its small size. In particular, an ACTH-secreting adenoma is so small that identifying the lesion is difficult with current imaging diagnostic methods. The minimal diameter for detecting ACTH-secreting microadenomas with MRI is about 2 to 3 mm.[17,18] Cavernous sinus sampling is useful in detecting the correct lateral orientation in laterally localized microadenomas when ACTH-secreting microadenomas are undetectable by MRI.[19] In the case of ectopic adenoma in the cavernous sinus or pituitary stalk, this sampling technique is unable to effectively identify the lesion; so that a new sensitive and specific technique for the diagnosis of microadenomas would be useful.

Positron emission tomography (PET) and SPECT are functional techniques and some studies with PET for pituitary adenomas have been reported.[20–22] Dopamine receptors, which are found in both normal glands and pituitary adenomas, have been studied with dopamine D2 receptor antagonists (C-11-raclopride and C-11-methylspiperone). These ligands have been found to be helpful in the initial PET evaluation of adenomas as well as in post therapy.

Fluorine-18-2-fluorodeoxyglucose (FDG) characterizes and measures energy metabolism covering a host of biologic activities such as cell proliferation, synaptic activity, hormonal proliferation and secretion, and glycosylation. In PET scans with FDG, the normal pituitary gland was not visible in any of the control subjects because of its small size and relatively low metabolic activity.[21] SPECT in combination with [^{111}In-DTPA-D-Phe]-octreotide is a recently developed technique for imaging somatostatin receptors in some pituitary adenomas.[23] These ligands accumulate in the normal or adenomatous pituitary gland based on the physical metabolic mechanism.

The mechanism for MIBI uptake in pituitary adenomas is not clear. MIBI is a lipophilic cationic complex that is sequestered within the cytoplasm and mitochondria of cells in relation to the negative potential of the inner mitochondrial and plasma membrane.[9] Because abundant mitochondria are generated in tissues with high aerobic metabolic activity, such as in endocrine tissues,[24] pituitary adenomas are considered to have higher cell viability than the normal pituitary gland. Although PET is a useful method in terms of functional imaging of the pituitary adenoma, it is too costly for many institutions.

MIBI-SPECT imaging is a useful technique for detecting adenomas and adenocarcinomas in the parathyroid and mammary glands. MIBI has also been reported to accumulate in both the normal pituitary gland and in adenomas.[11–13] There have no previous reports on the use of MIBI SPECT as a means for comparing the normal pituitary gland with pituitary adenoma. Evaluating MIBI uptake in the normal pituitary gland would be necessary for detecting abnormal uptake in microadenomas. In this study, MIBI was poorly taken up in the normal pituitary gland and not taken up at all in normal cerebral parenchyma. Instead, MIBI accumulated in the normal choroid plexus and salivary glands. This result corresponds with those reported previously.[6,27] Visual analysis showed that most of the longitudinal oval uptake was observed in macroadenomas but not in the normal pituitary gland, suggesting that macroadenomas grow longitudinally. On the registration image, the uptake shape corresponded to the form of the adenomas themselves. All triangular- or rectangular-shaped uptakes were observed in control subjects but not in pituitary adenoma patients. Distance analysis showed that uptake in the controls was located 3.8 mm (mean value) behind the uptake observed in the adenomas. MIBI uptake was found located behind the center of the sella turcica. This uptake was formed in relation to the shape of the dorsum sellae and the entire clivus. In this study, no uptake in the dorsum sellae or upper clivus was observed in pituitary adenoma patients. This result may be due to decalcification caused by compression of the adenoma or greater uptake in the adenoma than in the dorsum sellae and upper clivus. There were two types of uptake found in the controls. Circular uptake was found in the dorsum sellae and upper clivus, and triangular- or rectangular-shaped uptake was found in the entire clivus. It was necessary to observe the shape of the uptake by means of a midsagittal image because uptake in the dorsum sellae and upper clivus was often mistaken for uptake in the normal pituitary gland (Fig. 3). When the shape is circular and the uptake is hypoactive, SPECT imaging alone is insufficient to differentiate between the normal pituitary gland and microadenoma because the shape of uptake of the dorsum sellae and upper clivus adjoining the normal pituitary gland is similar to that in adenoma. In the present study, 5 of the control subjects and 6 microadenoma subjects had circular accumulation. The mean distances from the nasion to the uptake region on both MR and SPECT images were 68.2 ± 3.3 and 74 ± 4.3 respectively for the 5 controls and 68.2 ± 5.2 and 70.3 ± 5.2 respectively for the 6 microadenomas. Therefore, even with a circular SPECT image, the distinction between a normal gland and an adenoma can be made by measuring the distance from the nasion to the uptake region. MIBI SPECT could help in the diagnosis of suspected microadenomas where insufficient information is provided by MRI.

The mechanism of MIBI uptake in the dorsum sellae and clivus is unclear. Anatomically, the bone that forms the clivus is not considered to be a single bone from the viewpoint of embryology; rather the dorsum sellae and the upper clivus are part of the sphenoid bone. Bone marrow inside the clivus changes from red to yellow (fatty) marrow with age. Kimura et al.,[25] in their MRI study of a group of normal adults reported that normal clival marrow in 23% of the group was enhanced by gadopentetate-dimeglumine. Kimura et al. considered that a more homogeneous pattern of contrast enhancement within the marrow was presumably related to the contrast material pooling within the marrow sinusoids. Furthermore, enhancement might be observed more readily in red marrow, whereas the bright signal intensity of yellow marrow obscures contrast enhancement. In the present study, MIBI may have pooled in the dorsum sellae and clivus for similar reasons and regional uptake is due to hemodynamics that differ from that of MRI contrast material.

Recently a number of studies have been carried out on MIBI uptake in normal bone marrow and bone and soft tissue lesions.[26,27] According to animal experimental studies reported by Jonsson et al.,[15] approximately 80% of MIBI activity in normal skeletal tissue was found in red bone marrow. Homogeneously diffuse mild skeletal MIBI activity is a normal finding and not an indication of malignancy. Wakasugi et al.[26] observed an increase in homogeneously diffuse mild MIBI activity in the sternum and thoracic spine of 90 (73%) and 111 (90%) of 124 control patients with presumed normal bone and bone marrow. There have been no detailed reports on MIBI uptake in the cranial bone. The marrow in all cranial bones, however, is hematopoietic to some degree, although the proportions of red and yellow marrow vary.[28] We speculated that MIBI was pooling in the clivus and dorsum sellae, and it accumulated within the marrow sinusoids. SPECT imaging presumably demonstrated blood flow and/or metabolism of the bone marrow, and MRI indicated the degree of bone marrow conversion.

Superimposition is a useful technique when the shape of accumulation on the SPECT image is circular. Physiological function and organization metabolism can be evaluated with SPECT imaging, but SPECT is inferior to MRI in spatial resolution and shows only the distribution of radioisotope to a particular organization. It may be difficult to identify the location or size of a lesion based on SPECT imaging alone. To overcome this disadvantage, an attempt has been made to obtain diagnostic information by superimposing a SPECT image on to an MR image. There are two methods of registration, one with an artificial marker[29] and one with a patient's anatomical characteristics.[30] The approach to the latter method involves calculating the transformation matrix of coordinates in relation to scale, rotation and shift of the three axes in each of the image coordinate systems. In the present study we used the latter procedure to superimpose a SPECT image on an MR image. Because the pituitary gland is located on the midline of the skull, midsagittal plane imaging is adopted for both SPECT and MRI. Theoretically, when the two images are superimposed, two of the three axes will therefore fit together. Superimposition is completed by one axial rotation and shift while the enlargement ratios of the two images are matched. Additionally, anatomical features such as the nose, calvaria, and skull are based on the midsagittal plane aids image fitting. Fitting errors caused by rotation adjustments are though to be small because the pituitary gland is located close to the center of the skull.

It has been suggested that SPECT lesion detection rates are underestimated when the lesion size is smaller than twice the full width at half maximum.[31,32] Even though the FWHM introduced in this study was 8 mm, detection was still possible in microadenomas with diameters less than 10 mm. Microadenoma MIBI uptake was sufficient to allow SPECT detection and the adenoma itself would emit a large proportion of the scatter. This supports the concept that radioactivity of a pituitary adenoma depends upon not only adenoma uptake but also its scattering ability. MIBI SPECT may be helpful in diagnosing microadenoma that cannot be detected by MRI. The development of SPECT instruments and the introduction of tracers provide an alternative functional neuroimaging technique with the relative advantages of lower cost and clinical accessibility.

CONCLUSION

MIBI was taken up in the dorsum sellae or clivus but not the normal pituitary gland and had a strong affinity for pituitary adenoma. This result implies that MIBI SPECT may be a useful new auxiliary examination technique for location diagnosis of pituitary adenoma.

ACKNOWLEDGMENT

We are grateful to Dr. T. Kitamura and Dr. N. Sanno for their valuable advice concerning the design of this study.

REFERENCES

1. Nakahara H, Noguchi S, Murakami N, Hoshi H, Jinnouchi S, Nagamachi S, et al. Technetium-99m-sestamibi scintigraphy compared with thallium-201 in evaluation of thyroid tumors. *J Nucl Med* 1996; 37: 901–904.
2. Taillefer R, Boucher Y, Potvin C, Lambert R. Detection and localization of parathyroid adenomas in patients with hyperparathyroidism using a single radionuclide imaging procedure with technetium-99m-sestamibi (double-phase study). *J Nucl Med* 1992; 33: 1801–1807.
3. Yamamoto Y, Nishiyama Y, Satoh K, Takashima H, Ohkawa M, Fujita J, et al. Comparative study of technetium-99m-sestamibi and thallium-201 SPECT in predicting chemo-

therapeutic response in small cell lung cancer. *J Nucl Med* 1998; 39: 1626–1629.
4. Maublant J, de Latour M, Mestas D, Clemenson A, Charrier S, Feillel V, et al. Technetium-99m-sestamibi uptake in breast tumor and associated lymph nodes. *J Nucl Med* 1996; 37: 922–925.
5. Caner B, Kitapcl M, Unlu M, Erbengi G, Calikoglu T, Gogus T, et al. Technetium-99m-MIBI uptake in benign and malignant bone lesions: a comparative study with technetium-99m-MDP. *J Nucl Med* 1992; 33: 319–324.
6. O'Tuama LA, Treves ST, Larar JN, Packard AB, Kwan AJ, Barnes PD, et al. Thallium-201 versus technetium-99m-MIBI SPECT in evaluation of childhood brain tumors: a within-subject comparison. *J Nucl Med* 1993; 34: 1045–1051.
7. Sessler MJ, Geck P, Maul FD, Hor G, Munz DL. New aspects of cellular thallium uptake: Tl^+-Na^+-2Cl(−)-cotransport is the central mechanism of ion uptake. *Nuklearmedizin* 1986; 25: 24–27.
8. Sehweil AM, McKillop JH, Milroy R, Wilson R, Abdel-Dayem HM, Omar YT. Mechanism of ^{201}Tl uptake in tumours. *Eur J Nucl Med* 1989; 15: 376–379.
9. Chiu ML, Kronauge JF, Piwnica-Worms D. Effect of mitochondrial and plasma membrane potentials on accumulation of hexakis (2-methoxyisobutylisonitrile) technetium (I) in cultured mouse fibroblasts. *J Nucl Med* 1990; 31: 1646–1653.
10. Arbab AS, Koizumi K, Toyama K, Araki T. Uptake of technetium-99m-tetrofosmin, technetium-99m-MIBI and thallium-201 in tumor cell lines. *J Nucl Med* 1996; 37: 1551–1556.
11. Perez-Monte JE, Brown ML, Clarke MR, Watson CG, Carty SE. Parathyroid hyperplasia, thymic carcinoid and pituitary adenoma detected with technetium-99m-MIBI in MEN type I. *J Nucl Med* 1997; 38: 1767–1769.
12. Dierckx RA, Martin JJ, Dobbeleir A, Crols R, Neetens I, De Deyn PP. Sensitivity and specificity of thallium-201 single-photon emission tomography in the functional detection and differential diagnosis of brain tumours. *Eur J Nucl Med* 1994; 21: 621–633.
13. Soler C, Beauchesne P, Maatougui K, Schmitt T, Barral FG, Michel D, et al. Technetium-99m sestamibi brain single-photon emission tomography for detection of recurrent gliomas after radiation therapy. *Eur J Nucl Med* 1998; 25: 1649–1657.
14. Bagni B, Pinna L, Tamarozzi R, Cattaruzzi E, Marzola MC, Bagni I, et al. SPET imaging of intracranial tumours with ^{99}Tc^{m}-sestamibi. *Nucl Med Commun* 1995; 16: 258–264.
15. Jonsson C, Jacobsson H. Accumulation of ^{99m}Tc-MIBI in bone marrow. *Ann Nucl Med* 1996; 10: 281–285.
16. Bartynski WS, Lin L. Dynamic and conventional spin-echo MR of pituitary microlesions. *AJNR* 1997; 18: 965–972.
17. Colombo N, Loli P, Vignati F, Scialfa G. MR of corticotropin-secreting pituitary microadenomas. *AJNR* 1994; 15: 1591–1595.
18. Buchfelder M, Nistor R, Fahlbusch R, Huk WJ. The accuracy of CT and MR evaluation of the sella turcica for detection of adrenocorticotropic hormone-secreting adenomas in Cushing disease. *AJNR* 1993; 14: 1183–1190.
19. Teramoto A, Yoshida Y, Sanno N, Nemoto S. Cavernous sinus sampling in patients with adrenocorticotrophic hormone-dependent Cushing's syndrome with emphasis on inter- and intracavernous adrenocorticotrophic hormone gradients. *J Neurosurg* 1998; 89: 762–768.
20. Bergstrom M, Muhr C, Lundberg PO, Bergstrom K, Lundqvist H, Antoni G, et al. Amino acid distribution and metabolism in pituitary adenomas using positron emission tomography with D-[^{11}C]methionine and L-[^{11}C]methionine. *J Comput Assist Tomogr* 1987; 11: 384–389.
21. De Souza B, Brunetti A, Fulham MJ, Brooks RA, DeMichele D, Cook P, et al. Pituitary microadenomas: a PET study. *Radiology* 1990; 177: 39–44.
22. Bergstrom M, Muhr C, Lundberg PO, Langstrom B. PET as a tool in the clinical evaluation of pituitary adenomas. *J Nucl Med* 1991; 32: 610–615.
23. van Royen EA, Verhoeff NP, Meylaerts SA, Miedema AR. Indium-111-DTPA-octreotide uptake measured in normal and abnormal pituitary glands. *J Nucl Med* 1996; 37: 1449–1451.
24. Lloreta-Trull J, Serrano S. Biology and pathology of the mitochondrion. *Ultrastruct Pathol* 1998; 22: 357–367.
25. Kimura F, Kim KS, Friedman H, Russell EJ, Breit R. MR imaging of the normal and abnormal clivus. *Am Roentgenol* 1990; 155: 1285–1291.
26. Wakasugi S, Teshima H, Nakamura H, Hashizume T, Maeda T, Hiraoka A, et al. Tc-99m MIBI localization in bone marrow: a marker of bone marrow malignancy. *Clin Nucl Med* 1998; 23: 664–671.
27. Pace L, Catalano L, Pinto A, De Renzo A, Di Gennaro F, Califano C, et al. Different patterns of technetium-99m sestamibi uptake in multiple myeloma. *Eur J Nucl Med* 1998; 25: 714–720.
28. Hashimoto M. The distribution of active marrow in the bones of normal adult. *Kyushu J Med Sci* 1960; 11: 103–111.
29. Zhang J, Levesque MF, Wilson CL, Harper RM, Engel J Jr, Lufkin R, et al. Multimodality imaging of brain structures for stereotactic surgery. *Radiology* 1990; 175: 435–441.
30. van Herk M, Kooy HM. Automatic three-dimensional correlation of CT-CT, CT-MRI, and CT-SPECT using chamfer matching. *Med Phys* 1994; 21: 1163–1178.
31. Nakajima K, Hisada K, Iida H, Seki H, Muramori A. Detectability of small hot lesions in single photon emission computed tomography: experiments using phantom and computer simulation. *KAKU IGAKU (Jpn J Nucl Med)* 1987; 24: 397–405. (in Japanese)
32. Togawa T, Yui N, Kinoshita F, Yanagisawa M. Quantitative evaluation in tumor SPECT and the effect of tumor size: fundamental study with phantom. *Ann Nucl Med* 1997; 11: 51–54.